PCCP

Accepted Manuscript

ROYAL SOCIETY OF CHEMISTRY

www.rsc.org/pccp

ARTICLE TYPE www. rsc.org/xxxxxx | XXXXXXXX

Kinetics of the NH_3 and CO_2 solid-state reaction at low temperature.

Noble J. A.,[a] Theule P.,*[a] Duvernay F.,[a] Danger G.,[a] and Chiavassa T.[a]
Ghesquiere P.,[b] Mineva T., [c] and Talbi D.[b]

Received Xth XXXXXXXXXX 2014, Accepted Xth XXXXXXXXX 2014
First published on the web Xth XXXXXXXXXX 200X
DOI: 10.1039/b000000x

Ammonia and carbon dioxide play important roles in both atmospheric and interstellar ice chemistry. This work presents a theoretical and experimental study of the kinetics of the low-temperature NH_3 and CO_2 solid-state reaction in ice films, the product of which is ammonium carbamate ($NH_4^+NH_2COO^-$). It is a first-order reaction with respect to CO_2, with a temperature-dependent rate constant fitted to an Arrhenius law in the temperature range 70 K to 90 K, with an activation energy of 5.1 ± 1.6 kJ.mol^{-1} and a pre-exponential factor of $0.09\ ^{+1.1}_{-0.08}$ s^{-1}. This work helps to determine the rate of removal of CO_2 and NH_3, via their conversion into ammonium carbamate, from atmospheric and interstellar ices. We also measure first-order desorption energies of 69.0 ± 0.2 kJ.mol^{-1} and 76.1 ± 0.1 kJ.mol^{-1}, assuming a pre-exponential factor of 10^{13}s^{-1}, for ammonium carbamate and carbamic acid, respectively.

1 Introduction

Ammonia (NH_3) and carbon dioxide (CO_2) are ubiquitous constituents of the Earth's atmosphere and of the molecular interstellar medium.

On Earth, ammonia is considered to be the most important of all nitrogen-bearing species which are deposited onto vegetation and other receptors[1]. Ammonia originates from animal waste and the volatilisation of synthetic fertilizers, biomass burning, losses from soils bearing native vegetation or agricultural crops, and fossil fuel combustion[2]. Ammonia is a very important alkaline constituent in the atmosphere as it reacts readily with acidic substances, *e.g.* sulfuric acid (H_2SO_4) or nitric acid (HNO_3), to form ammonium (NH_4^+) salt aerosols[1]. The removal of gaseous NH_3 from the atmosphere by the formation of fine particulate NH_4^+ salts is a very efficient mechanism. The effects of NH_3 when combined with other air pollutants, such as the all-pervasive ozone (O_3) or the increasingly abundant carbon dioxide (CO_2), are poorly understood. Atmospheric CO_2 is of prime importance in plant and algal photosynthesis, as well as the greenhouse effect. It originates from the respiration processes of living aerobic organisms, organic matter, and volcanic outgassing. Its increasing concentration contributes to global warming and ocean acidification. Its chemical capture through conversion into non-volatile species is a vast field of research[3]. Plants naturally fix the CO_2 they need for their growth in the form of a carbamate using the ribulose 1,5-bisphosphate carboxylase/oxygenase enzyme in the first step of the Calvin cycle[3]. It is therefore important to understand how the reactivity between NH_3 and CO_2 can lead to other Non Methane Volatile Organic compounds (NMVOC) or refractory species on aerosols or in terrestrial ice. The reaction of carbon dioxide with Bronsted bases is of great importance in biology, geology, and for industrial applications[4]. As an example, amines (RNH_2) are used to remove carbon dioxide from gas streams[5].

In space, water, carbon dioxide, and ammonia are among the most abundant species present in interstellar ices. They are formed during the transition from the diffuse atomic medium to the dense molecular medium via simple atomic or diatomic reactions on the surface of bare interstellar grains. Ammonia is formed by the hydrogenation of the N atom[6]. Carbon dioxide is thought to be formed from the HO-CO complex[7–9] or by the addition reaction CO + O[10]. Water can be formed by the hydrogenation of the O atom, O_2 or O_3 molecules, or the OH radical[11–15]. In molecular clouds and in solar system bodies, carbon dioxide and ammonia have abundancies on the order of 20 % and 5 %, respectively[16]. Under interstellar conditions, both molecules are transformed into other species either thermally[17–20] or non-thermally, due to the effect of UV photon irradiation[21], proton or heavy ion bombardment[22,23], and/or electron bombardment[24]. Products will either enrich the gas-phase of the interstellar medium in complex organic

[a] *Aix-Marseille Univ., PIIM UMR 7345, 13397, Marseille, France CNRS, PIIM UMR 7345, Marseille, 13397, France; Tel: +33 4 91 28 85 82;*
[b] *Laboratoire Univers et Particules de Montpellier UMR 5299, CNRS et Université Montpellier 2, Place Eugène Bataillon, 34095 Montpellier cedex 05, France.*
[c] *Institute Charles Gerhardt, Montpellier, UMR 5253 CNRS/ENSCM/UM2/UM1, 8 rue de l'Ecole Normale, 34296 Montpellier cedex 05, France.*
* E-mail: patrice.theule@univ-amu.fr

molecules when the ice mantle is desorbed or be a constituent of the refractory organic residue.

In this work we investigate the reaction mechanisms and the kinetics of the NH_3:CO_2 solid-phase system, with the reactants located on neighboring sites. Low-temperature NH_3:CO_2 thermal reactivity has been shown to lead to the formation of the ammonium carbamate salt ($[NH_4^+][NH_2COO^-]$), carbamic acid (NH_2COOH)[17–20] and, in the presence of water, the ammonium bicarbonate salt ($[NH_4^+][HCO_3^-]$)[20]. While these previous works spectroscopically characterise the reaction products, the mechanisms and the kinetics of the reaction NH_3 + CO_2 have not yet been addressed experimentally. High level calculations on the solvation of CO_2 in water-ammonia clusters of four molecules are reported[25], with barriers of solvation determined at between 60 and 110 kJ.mol^{-1}. Here, we present the results of dedicated isothermal laboratory experiments on NH_3:CO_2 ice films of different concentration ratios, measured using Fourier Transform Infrared Spectroscopy (FTIR). We measured the reaction barrier to the formation of ammonium carbonate to be E_a^{th}= 5.1 kJ.mol^{-1} ± 1.6 kJ.mol^{-1}. The substitution of a NH_3 molecule by a H_2O molecule is also investigated. The question of the diffusion of the reactants within the ice has been purposefully separated from the reactivity of the reactants, and will be addressed in a future publication (Ghesquiere *et al*, *in preparation*). We also performed calculations based on density functional theory to mimic the reaction of NH_3 and CO_2 in a water/ammonia cluster to aid the interpretation of experimental results and to provide insight into the mechanism(s) for the formation of ammonium carbamate ($NH_4^+NH_2COO^-$) and carbamic acid (NH_2COOH) in a model NH_3:CO_2:H_2O ice mixture.

Reaction mechanisms:

The formation of the products NH_2COOH (A) and $NH_4^+NH_2COO^-$ (C) from the reactants NH_3 and CO_2 can occur via three mechanisms.

In the first mechanism, NH_2COOH is a reaction intermediate, and $NH_4^+NH_2COO^-$ the final product, of a sequence of two successive reactions:

$$NH_3 + CO_2 \rightleftharpoons NH_2COOH \quad (1)$$
$$NH_3 + NH_2COOH \rightleftharpoons NH_4^+NH_2COO^- \quad (2)$$

In a second mechanism, the reaction pathway proceeds via a zwitterion ($NH_3^+COO^-$, Z) intermediate, rather than carbamic acid:

$$NH_3 + CO_2 \rightleftharpoons NH_3^+COO^- \quad (3)$$
$$NH_3 + NH_3^+COO^- \rightleftharpoons NH_4^+NH_2COO^-. \quad (4)$$

If we are not able to observe the zwitterion intermediate, it can not be included in the kinetic analysis and thus we can not distinguish between reactions 1 and 3.

In the third mechanism, $NH_4^+NH_2COO^-$ is produced as a reaction intermediate (either directly or via a zwitterion, as in the second mechanism); NH_2COOH is the final product of a sequence of two successive reactions:

$$2NH_3 + CO_2 \rightleftharpoons NH_4^+NH_2COO^- \quad (5)$$
$$NH_4^+NH_2COO^- \rightleftharpoons NH_3 + NH_2COOH \quad (6)$$

2 Methods

2.1 Experimental methods

The experiments were performed using our RING experimental set-up, as described elsewhere[26]. A gold-plated copper surface in a high-vacuum chamber (few 10^{-9} mbar) is held at low temperature using a closed-cycle helium cryostat (ARS Cryo, model DE-204 SB, 4 K cryogenerator). The sample temperature is measured using a DTGS 670 Silicon diode with an uncertainty of 0.5 K. The temperature is controlled using a Lakeshore Model 336 temperature controller and a heating resistance. Infrared absorption spectra are recorded in reflection mode by means of Fourier-transform infrared reflection absorption spectroscopy (or FTIR) using a Vertex 70 spectrometer with either a DTGS detector or a liquid N_2-cooled MCT detector. A typical spectrum has a 0.5 cm^{-1} resolution and is averaged over a few tens of interferograms. Mass spectra of the gas-phase species are recorded using a Hiden HAL VII RGA quadrupole mass spectrometer (QMS). The ionization source is a 70 eV impact electronic source. Mass spectra are recorded between 1 and 60 amu.

NH_3:CO_2(:H_2O) ice films are formed by vapour deposition. Gas-phase CO_2 and NH_3 are commercially available in the form of 99.9995 % pure gas from Linde and Air Liquide, respectively. The H_2O vapour is obtained from deionised water which has been purified by several freeze-pump-thaw cycles, carried out under primary vacuum. The different gases are inserted and mixed together in a defined concentration ratio in a primary pumped vacuum line using standard manometric techniques at room temperature. The homogeneously mixed gas-phase mixture is then sprayed onto the cold gold-plated copper surface.

The morphology of the NH_3:CO_2(:H_2O) ice film depends on the temperature of the gold surface the gas-phase mixture is deposited onto[27]. If the ice film is deposited below 60 K, the ice film is amorphous and porous. If deposited between 60 K and 150 K, the ice is amorphous and compact, with little or no porosity. If deposited above 150 K, the ice is crystalline. We deposit the homogeneous NH_3:CO_2 gas-phase mixture at 60 K in order to measure the NH_3 + CO_2 reactivity in compact amorphous ice. Such ice films are better defined and more re-

producible than porous amorphous ice films. Pore collapse in the latter can change the overall kinetics by introducing additional reorganisation kinetics[28].

The column density (N, molecules.cm^{-2}) of each molecular species is derived immediately after deposition from the IR spectra, an example of which is presented in Fig. 1(a), using the expression:

$$N = \frac{\int \tau_\nu d\tilde{\nu}}{A}, \quad (7)$$

where optical depth (τ_ν) is equal to ln(10) times the integrated absorbance, and A is the band strength, in cm.molecule^{-1}. Ammonia is identified via its umbrella mode at 1110 cm^{-1}, the band strength of which is 1.3 10^{-17} cm.molecule^{-1} [29]. Carbon dioxide is identified via its asymmetric stretching mode at 2339 cm^{-1} and its bending mode band at 667 cm^{-1}. The band strength for the CO_2 asymmetric stretching band was measured as 7.6 10^{-17} cm.molecule^{-1} for the pure solid[30,31], while in water ice, a value of 1.4 10^{-17} cm.molecule^{-1} was found[32]. Water ice has three characteristic bands at 3280, 1660, and 760 cm^{-1} corresponding to the OH stretching, HOH bending, and libration modes, respectively. The corresponding band strengths are 2.1 $\times$10^{-16}, 3.1 $\times$10^{-17}, and 3.1 $\times$10^{-17} cm.molecule^{-1}, respectively[31]. The frequencies and band strengths for the carbamate are taken from Bossa et al.[19]. There is an approximately 30 % uncertainty on the band strengths and therefore on the calculated column densities. The characteristic frequencies of the different products are listed in Table 1 .

Table 1 Infrared absorption bands and assignments of the products formed from the NH_3 + CO_2 reactivity.

assignment	wavenumbers (cm^{-1})
$\nu(NH_2)$ NH_2COOH dimer	3462
$\nu(NH_2)[NH_4^+][NH_2COO^-]$	3428
$\nu(NH_2)[NH_4^+][NH_2COO^-]$	3325
$\nu(OH)$ NH_2COOH	3140 *
$\nu(C=O)$ NH_2COOH	1691
$\delta(NH_2)[NH_4^+][NH_2COO^-]$	1623
$\nu_{as}(COO^-)[NH_4^+][NH_2COO^-]$	1553
$\delta(NH_4^+)[NH_4^+][NH_2COO^-]$	1495
NH_2COOH dimer	1451
$\nu(CN)$ $[NH_4^+][NH_2COO^-]$	1393
NH_2COOH dimer	1320
$\nu_s(COO^-)$ $[NH_4^+][NH_2COO^-]$	1117
$\rho(NH_2)$ $[NH_4^+][NH_2COO^-]$	1037
$\delta_{oop}(OCN)$ $[NH_4^+][NH_2COO^-]$	829
$\delta(COO^-)$ $[NH_4^+][NH_2COO^-]$	674

* broad band

The ice film thickness is determined from the measured column density (N, molecule.cm^{-2}), assuming ρ=0.94 g.cm^{-3} as the amorphous ice density, and using:

$$l_{[cm]} = \frac{N \times 17}{\rho \times N_A} \times cos(18^o)/2, \quad (8)$$

where N_A is the Avogadro constant, 17 g.mol^{-1} is the molar mass for NH_3, and the cos(18^o) term comes from the 18^o incidence angle between the FTIR beam and the normal to the ice film. The factor one half comes from the reflection mode, which probes double the column density.

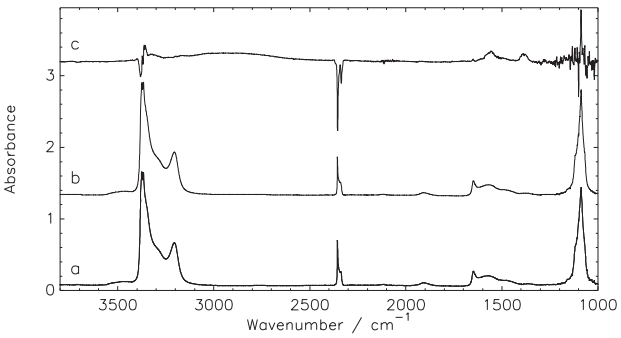

Fig. 1 Infrared absorption spectra of an homogeneously mixed NH_3:CO_2 ice film with an excess of NH_3 held at 80 K. Spectra are: (a) at t= 0, (b) after 11 hours at 80 K , and (c) the difference spectrum of (b) minus (a) magnified by a factor of 10. The CO_2 bands have decreased while the carbamate bands have appeared.

We use two approaches to derive the relevant physical and chemical parameters of the NH_3:CO_2 system:

- During isothermal kinetic (IK) experiments, infrared spectra of the solid-phase molecules are taken at regular time intervals at a fixed temperature.
- During temperature ramp experiments, IR spectra of the solid-state molecules are taken at regular time (temperature) intervals, and mass spectra of the gas-phase molecules are taken as they desorb during a temperature ramp.

2.1.1 Isothermal kinetic experiments:

In isothermal kinetics (IK) experiments, immediately after deposition the ice film is heated as fast as possible to a fixed temperature (T), in typically a few tens of seconds. Once the temperature, T, is reached, we set the initial time, t = 0 s, of our isothermal experiment. NH_3 and CO_2 react to form reaction products, as can be seen from the IR spectrum and the difference spectrum of the ice mixture at the end of the experiment, as displayed in Fig. 1(b) and (c). The kinetics of the NH_3 + CO_2 ice mixture at the fixed temperature, T, are monitored by measuring the disappearance of the reactants and appearance of the products from their characteristic IR

absorption bands as a function of time, as illustrated for a typical isothermal experiment in Fig. 2. Isothermal kinetics experiments are performed at different temperatures to study the temperature dependence of the reactivity. These kinetics will determine the removal of NH_3 and CO_2 in atmospheric or interstellar ices. Since both in atmospheric and interstellar chemistry this reaction is competing with other reactions, such as NH_3 + HNCO[28], NH_3 + H_2CO[33], or CH_3NH_2 + CO_2[34], it is important to know its kinetic parameters in order to compare it with the other reactions.

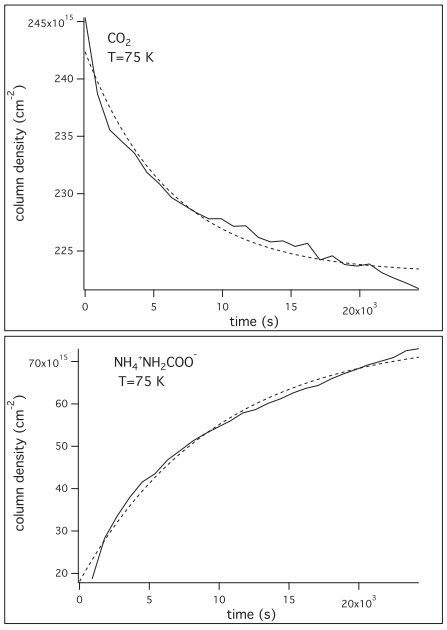

Fig. 2 Isothermal kinetic experiments at 75 K on an homogeneously mixed NH_3:CO_2 ice film, deposited at 60 K with an excess of NH_3 (solid lines). The CO_2 column density exponentially decreases with time as the $NH_4^+COO^-$ (from its band at 1393 cm^{-1}) increases (dashed lines).

The temperature range within which isothermal experiments can be performed is limited. The lowest temperature is constrained by the maximum time we can wait. This time is defined by the amount of background deposition onto the ice film from the vacuum chamber; at 10^{-8} mbar, *c.a.* 360 monolayers are deposited in 10 hours. The highest temperature is constrained by the desorption of our ice film. With pre-exponential factors of 5 $10^{13}s^{-1}$ and 6 $10^{14}s^{-1}$ and desorption energies of 25 and 23 kJ.mol^{-1} for NH_3 and CO_2, respectively[35,36], the desorption rates of NH_3 and CO_2 can be evaluated. For example at 80 K, it takes approximately seven minutes to desorb one monolayer.

2.1.2 Temperature ramp experiments:

In temperature programmed reactivity (TPR) experiments, the temperature is linearly increased at a ramp rate, β, from the deposition temperature, T_0:

$$T = T_0 + \beta \times t. \quad (9)$$

The abundances of the solid-phase species during the temperature ramp are measured from FTIR spectra.

In temperature programmed desorption (TPD) experiments, the temperature is also linearly increased, as in Eq. 9. During heating, the mass spectrum of the sublimating species is recorded; desorption parameters are derived from TPD experiments.

2.2 Computational methods

Energy profile calculations have been performed within the framework of Density Functional Theory using the hybrid generalised gradient approximation (GGA) B3LYP functional[37,38] in conjunction with a triple zeta atomic basis set extended by polarisation functions i.e., 6-311G(d,p). Structures at minima and maxima (transition states) on the reaction paths have been located by total optimisation using analytical gradients. Harmonic vibrational analyses have been performed at the same levels of theory to confirm each stationary point as either an equilibrium structure (i.e., all real frequencies) or a transition structure (TS) (i.e., with one imaginary frequency). Intrinsic reaction coordinate calculations have been conducted in order to reliably link the transition states with corresponding minima. All energies have been corrected for unscaled zero-point energies calculated at the same theoretical level. All calculations have been performed using the GAUSSIAN-09 package[39].

3 Results

3.1 Experimental results

We perform several IK and TPR experiments at different temperatures on several CO_2:NH_3 ice mixtures with varying concentration ratios to investigate the reaction mechanism and measure the kinetics of the reaction. First we study the reactivity in a non protic CO_2 dominated ice, and second in a protic NH_3 dominated ice. The possible influence of H_2O is addressed.

3.1.1 Reactivity of the NH_3:CO_2 system with CO_2 in excess:

In NH_3:CO_2 ice mixture with a 1:20 concentration ratio, where NH_3 is diluted in a CO_2 ice, no reactivity is observed at any temperature below the desorption temperature of CO_2. This means that the reaction barriers are too high and, as a result, the desorption of CO_2 is faster than any reaction. This

case, where ice is dominated by a non-polar molecule such as CO_2, is less usual in real ices, which are usually water-dominated. Thus we will focus on NH_3:CO_2 where polar and hydrogen bonded molecules, such as NH_3 and H_2O, are dominant.

3.1.2 Reactivity of the NH_3:CO_2 system with NH_3 in excess:

We perform TPR experiments on NH_3:CO_2 ice films deposited at 60 K and heated at different temperature ramp rates, as shown in Fig. 3. The characteristic IR bands of $NH_4^+NH_2COO^-$ increase as it is produced and decrease as it sublimates. NH_2COOH is not identified in our spectra, either as a transitory species or as a final product, when NH_3 is in excess. Indeed, carbamic acid is observed in TPR experiments, at high temperatures, only when CO_2 is present at equal concentration with NH_3, as previously shown[19,20]. The absence of NH_2COOH tends to validate either the second mechanism, with a non-observable zwitterion intermediate, where the activation energy of reaction 4 is lower than that of reaction 3, or the third mechanism, a serial formation pathway of NH_2COOH from $NH_4^+NH_2COO^-$, the second step (reaction 6) having too large an energy to occur before carbamate desorption.

Thus, the experimental observations can be summarised as:

$$2NH_3 + CO_2 \rightleftharpoons NH_4^+NH_2COO^- \qquad (10)$$

We assume the reaction can be described using kinetic equations of the form:

$$\begin{aligned} \frac{d(CO_2)}{dt} &= -k(T) \times (NH_3)^{\alpha} \times (CO_2)^{\beta} \\ \frac{d(NH_4^+NH_2COO^-)}{dt} &= k(T) \times (NH_3)^{\alpha} \times (CO_2)^{\beta} \end{aligned} \qquad (11)$$

where k(T) is the temperature-dependent reaction rate constant, α and β are the partial orders of reaction, and (X) the molar fraction of the X species (with no dimension). In the case of excess NH_3, $(NH_3) \simeq 1$ and we measure an effective reaction rate constant of $k' = k(T) \times (NH_3)^{\alpha}$.

In NH_3:CO_2 ice mixtures where CO_2 is diluted in an excess of NH_3, each CO_2 molecule is surrounded by a NH_3 molecular environment and we can assume pseudo first-order kinetics for every reaction. The NH_3:CO_2 ice films are deposited at 60 K. IR bands of reactants decrease and product bands increase as the temperature is increased, which implies that NH_3 and CO_2 react.

3.1.2.1 Determination of the partial orders of reaction: Isothermal kinetic experiments on NH_3:CO_2 ice films with an excess of NH_3 exhibit a time dependence, with CO_2 and $NH_4^+NH_2COO^-$ concentrations evolving as depicted in Fig. 2. The exponential decay of CO_2 and the corresponding growth of $NH_4^+NH_2COO^-$ exhibit pseudo first-order reaction kinetics, with a rate constant k', *i.e.* β=1. The system of kinetic equations 11 is solved analytically as:

$$(CO_2)(t) = (CO_2)_0 \times e^{-k't} \qquad (12)$$

$$(NH_4^+NH_2COO^-)(t) = (CO_2)_0(1 - e^{-k't}). \qquad (13)$$

Fitting IK experiments with Eqns 12 and 13 gives the pseudo first-order reaction constant, k', at the fixed temperature T. To determine the partial reaction order, α, we measure k' at different (NH_3) molar fractions for the same temperature, as shown in Table 2 and in Fig. 4. The pseudo first-order reaction constant k' shows no dependence on the NH_3 molar fraction, which indicates that $\alpha = 0$ and therefore that k'=k. Due to the relatively large uncertainties on our measurements, the determination of α is tentative. In this particular case, the unit of k is s^{-1}.

3.1.2.2 Determination of the temperature dependence of the reaction rate:

In order to determine the temperature dependence of the reaction rate constant k(T), different IK experiments are performed at different fixed temperatures. They are summarised in Table 2.

The temperature dependence of the pseudo first-order reaction rate constant, k, is determined from the values for mixtures with an excess of NH_3 in Table 2, and is displayed in Fig. 5. The uncertainties are evaluated by (*i.*) taking into account the fitting uncertainty on each fitting procedure, (*ii.*) the

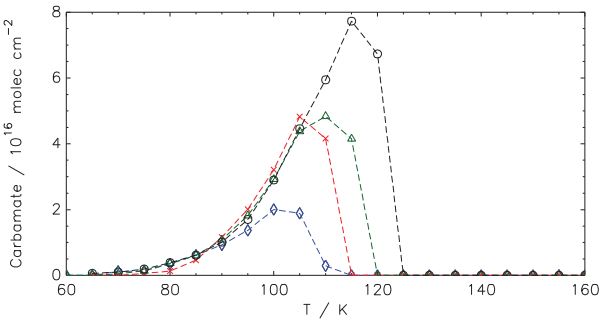

Fig. 3 $NH_4^+NH_2COO^-$ produced during Temperature Programmed Reactivity experiments on NH_3:CO_2 ice mixtures with an excess of NH_3. The temperature is ramped between 60 K and 160 K at rates of 0.5 (diamonds), 1 (crosses), 2 (triangles) and 5 (circles) K.min^{-1}. $NH_4^+NH_2COO^-$ abundances are monitored using the 1393 cm^{-1} band. IR bands corresponding to NH_2COOH are not observed when NH_3 is in excess. Although the initial quantity of matter (the curve area) is different in the four experiments, the slope of the curves is the same.

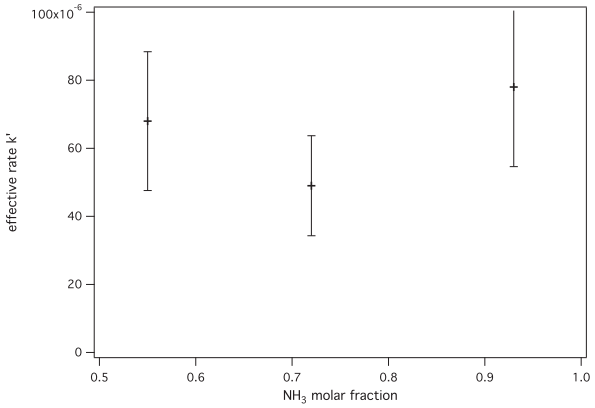

Fig. 4 Dependence of the pseudo first-order reaction constant $k' = k \times (NH_3)^{\alpha}$ on the (NH_3) molar fraction at T= 80 K. We limit (NH_3) to approximately 0.66, since we need at least two NH_3 molecules to react with one CO_2 molecule.

dispersion on the rate constants obtained from the CO_2 band and from the four carbamate bands, and (*iii.*) from the dispersion on two experiments performed at the same temperature. The uncertainty is dominated by the dispersion, which results from the pore collapse of the out-of-equilibrium ice[28]. The uncertainty on the temperature measurement is 0.5 K.

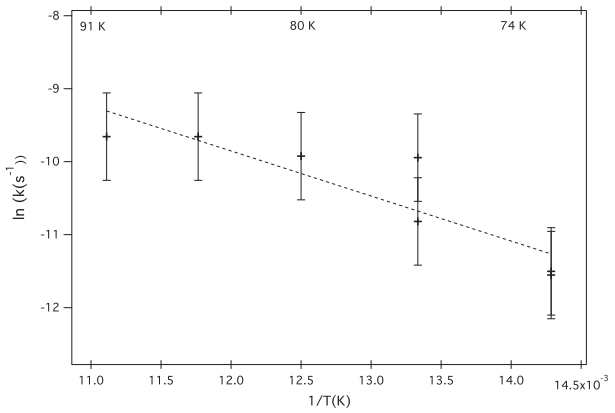

Fig. 5 Logarithm of the pseudo first-order reaction rate constant, k, as a function of the inverse of the temperature. The uncertainty on each point is estimated from both the fitting procedures for the CO_2 band and the four carbamate bands time decay, and from the dispersion between two measurements taken at 70 K and 75 K.

Fitting the experimental curve with an Arrhenius law gives an experimental activation energy of 5.1 ± 1.6 kJ.mol^{-1} (642 ± 62 K) and a pre-exponential factor of 0.09 $^{+1.1}_{-0.08}$ s^{-1} for a temperature interval between 70 K and 90 K. The small value of the pre-exponential factor can have two origins: either the measured pseudo first-order rate represents a sequence of elementary processes, or there is a contribution from quantum tunnelling between 70 K and 90 K[40]. Such a quantum tunnelling effect has been observed at lower temperature (8 – 15 K) in the HNCO + NH_3 system[28] (although not in the HNCO + H_2O system[26]) and it contributes to the reaction rate in the range 15 – 40 K, along with the thermal reaction rate. The latter takes over as the reaction temperature increases.

Table 2 Reaction rate constants, k, from isothermal experiments with different NH_3:CO_2 concentration ratios. Uncertainties on the last digit of the rates are in parenthesis.

CO_2:NH_3 ice films		
T(K)	concentration ratio	rate constant k' (s^{-1})
70-95	excess of CO_2	no reaction
70	excess of NH_3	9.6(2) 10^{-6}
70	excess of NH_3	1.0(1) 10^{-5}
75	excess of NH_3	4.8(3) 10^{-5}
75	excess of NH_3	2.0(5) 10^{-5}
80	excess of NH_3	4.9(3) 10^{-5}
85	excess of NH_3	6.4(4) 10^{-5}
90	excess of NH_3	6.4(4) 10^{-5}
80	1:1	6.8(5) 10^{-5}
80	1:4	4.9(4) 10^{-5}
80	1:13	7.8(5) 10^{-5}
CO_2:NH_3:H_2O ice films		
T(K)	concentration ratio	rate constant k' (s^{-1})
80	1:60:60	5.8(4) 10^{-5}
80	1:60:60	9.0(4) 10^{-5}

3.1.3 Determination of the influence of H_2O:

In order to investigate the change in reactivity induced by replacing a NH_3 molecule by a H_2O molecule, including its possible effect on the height of the reaction barrier, we perform IK experiments on CO_2:NH_3:H_2O ice films with different NH_3:H_2O ratios. We take care not to go below a 1:1 ratio, since we need at least two NH_3 molecules in the four closest neighbouring molecules of the first shell around CO_2 to form $NH_4^+NH_2COO^-$. If no NH_3 molecule is present in the first shell, it needs to diffuse toward CO_2 through the H_2O molecules, which alters the kinetic measurements. We see in Table 2 that the rates at 80 K are, within the dispersion uncertainty, similar or slightly higher if NH_3 molecule is replaced by a H_2O molecule. This means that, within the dispersion of our experimental methods, NH_3 and H_2O have more or less the same effect on the reaction barrier.

In the presence of water, the formation of ammonium bicarbonate $NH_4^+HCO_3^-$ can also take place[25].

$$NH_3 + CO_2 + H_2O \rightleftharpoons NH_4^+HCO_3^- . \qquad (14)$$

We do not observe the formation of ammonium bicarbonate in our experiments, perhaps due to the limited range of temperature.

3.1.4 Reactivity of the CO_2:NH_3 system with equal amounts of CO_2 and NH_3:

When CO_2 and NH_3 are present in comparable amounts in ice films, both ammonium carbamate and carbamic acid are formed [19,20].

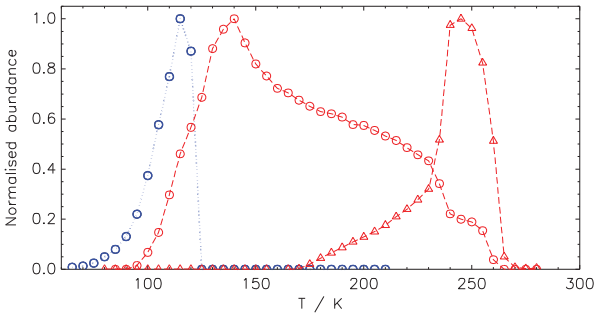

Fig. 6 A temperature programmed reactivity experiment performed at 5 K.min^{-}1 on a CO_2:NH_3 ice mixture in a 1:1.5 concentration ratio after an isothermal experiment at 80 K lasting 26.75 hours. The evolution of $NH_4^+NH_2COO^-$ (circles, dashed line) and NH_2COOH (triangles, dashed line) is monitored via their bands at 1393 cm^{-1} and 3462 cm^{-1} cm^{-1}, respectively, when the temperature is ramped between 60 K and 300 K. The (blue) dotted line (circles) is a TPR experiment performed immediately after the CO_2:NH_3 ice mixture deposition (data from Figure 3, 5 K.min^{-}1, circles). The desorption of reactants prevents the formation of large quantities of carbamate, and consequently of carbamic acid as well.

We see in Fig. 6 that ammonium carbamate ($NH_4^+NH_2COO^-$) forms first, and that carbamic acid (NH_2COOH) forms later from the carbamate. Above 150 K, the CO_2 and NH_3 initial reactants have desorbed and are not present anymore. Part of the formed carbamate has co-desorbed with them. Above 150 K the ice film is made of carbamate only and carbamate is converted into carbamic acid, as seen in Fig. 6 between 150 K and 225 K. Above 225 K, both the carbamate and carbamic acid desorb. These experiments clearly show that we have an additional high-temperature mechanism of conversion of the carbamate into carbamic acid:

$$NH_4^+NH_2COO^- \rightleftharpoons NH_3 + NH_2COOH. \qquad (15)$$

This is consistent with reaction 6 of the third reaction mechanism, although it could also be the reverse reaction of reaction 2.

3.1.5 Determination of the desorption energy of ammonium carbamate and carbamic acid:

To determine the desorption parameters of ammonium carbamate, we perform a TPD experiment on a CO_2:NH_3 ice mixture with an excess of NH_3. The mixture was held at 75 K for 12 hours in an IK experiment, then the temperature was ramped at a rate of 5 K/min. The TPD profile of m/z 44 displayed in Fig. 7 shows three desorption features, which can be assigned from the correlation with IR bands. The first feature at 120 K corresponds to the desorption of CO_2 [36,41] which did not react with NH_3. The second feature at 240 K corresponds to the desorption of $NH_4^+NH_2COO^-$. The third feature at 265 K corresponds to the desorption of NH_2COOH.

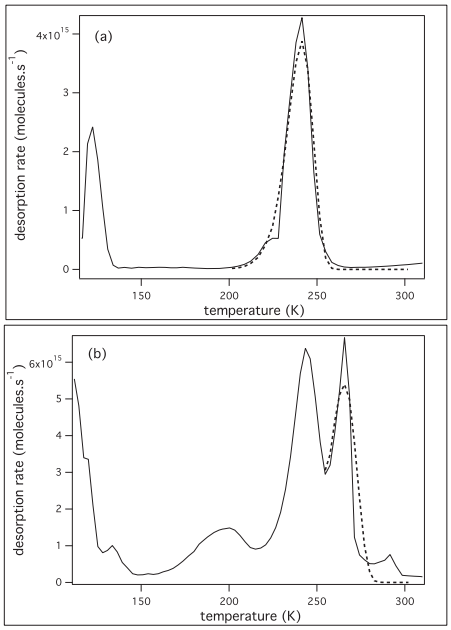

Fig. 7 Temperature programmed desorption experiment (m/z 44) at a 5 K/min temperature ramp of (a) a CO_2:NH_3 ice mixture with an excess of NH_3, and (b) an approximately equal amount of CO_2 and NH_3. The shoulder on the desorption feature is due to the crystallisation. The first desorption feature at 120 K corresponds to CO_2 desorption, the second one at 240 K to NH_4^+:NH_2COO^- desorption, and the third one at 265 K to NH_2COOH desorption, according to their correlation with IR bands. Fitting the experimental curve with a first-order Polanyi-Wigner equation (dashed line) gives the desorption parameters of NH_4^+:NH_2COO^- and of NH_2COOH.

Replacing time by temperature, using Eq. 9, in the Polanyi-Wigner equation, we get:

$$\frac{N}{dT} = -\frac{\nu}{\beta} \exp -E_{des}RT \times N^n, \qquad (16)$$

where ν and E_{des} are the pre-exponential factor and desorption energy of the desorption rate constant, and n is the order of the desorption. Fitting the carbamate desorption feature at 240 K with a first-order Polanyi-Wigner equation while fixing the pre-exponential factor to a typical value of ν=10^{13} s^{-1}, we get E_{des}=69.0 $\pm$ 0.2 kJ.mol^{-1}. Fitting the carbamic acid desorption feature at 265 K with a zeroth-order Polanyi-Wigner

equation while fixing the pre-exponential factor to a typical value of ν=10^{13} s^{-1}, we get E_{des}=76.1 ± 0.1 kJ.mol^{-1}. The higher desorption energy of carbamic acid is probably due to its ability to arrange into dimers [19].

Figure 8 shows the mass spectrum of ammonium carbamate and carbamic acid at their maximum desorption temperatures, *i.e.* 240 K and 265 K, respectively. For carbamic acid, the molecular ion at m/z 61 is weak but detectable and masses m/z 17, 18, and 44, corresponding to NH_3 and CO_2, dominate. Carbamic acid decomposes into NH_3 and CO_2 either spontaneously or under electron impact, but is stable for at least some time since the molecular ion at m/z 61 is observed. For ammonium carbamate, the molecular ion at m/z 78 is not observed, but rather m/z 61, corresponding to NH_2COOH, is weakly observed, and the masses corresponding to NH_3 and CO_2 dominate. The carbamate decomposes in the gas phase, either spontaneously or under the electron impact, into NH_3 and NH_2COOH and then into NH_3 and CO_2.

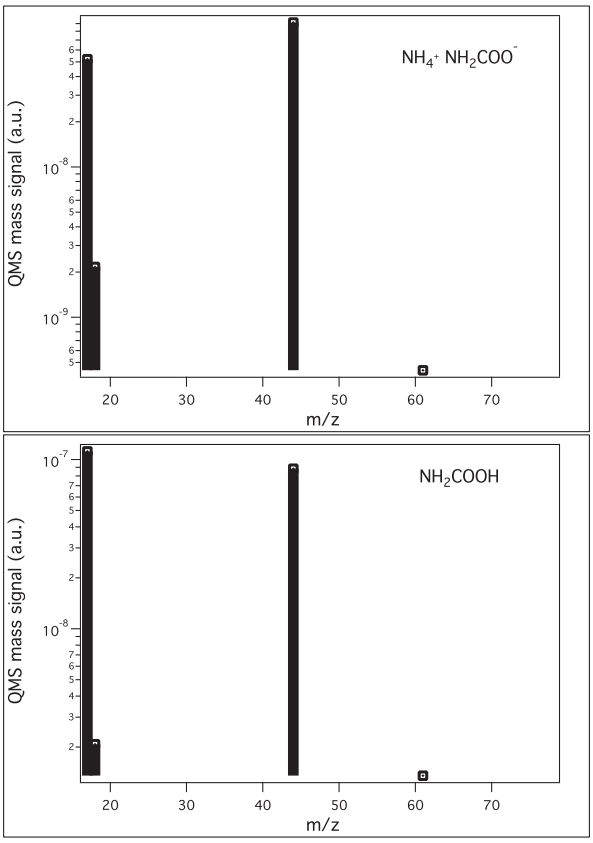

Fig. 8 Mass spectrum of ammonium carbamate (NH_4^+:$NH_2CH_2COO^-$) at T= 240 K (top) and of carbamic acid (NH_2COOH) at T=265 K (bottom) obtained using a QMS spectrometer with a 70 eV electron impact source.

3.2 Theoretical results

Three different clusters of eight molecules were constructed in order to study the reactivity of NH_3 and CO_2 in water : ammonia environments. These clusters were designed to provide a fully solvated first solvation layer (*i.e.* six molecules around the NH_3-CO_2 pair). Such cluster calculations are inherently gas phase calculations and thus resemble the energetics of the solid state reaction only approximately, independent of the quantum chemical method / DFT functional used.

The first cluster was designed to mimic the reactivity of CO_2 and NH_3 in a pure ammonia ice, and therefore it was constructed from one CO_2, and seven NH_3 molecules. This cluster is labeled "7:1:0", derived from the NH_3:CO_2:H_2O concentration ratio. The two other clusters were designed to mimic the reaction of NH_3 and CO_2 in a diluted, water-dominated environment. One was composed of one CO_2, one NH_3, and six H_2O molecules, hereafter "1:1:6". The other was composed of one CO_2, two NH_3, and five H_2O molecules, hereafter "2:1:5".

We would like to point out here that our goal with these calculations is not to provide accurate energy barriers, but rather to compare different mechanism in order to assess the catalytic role of ammonia and water molecules in the formation of ammonium carbamate and carbamic acid in model ices, and thus to rationalise the present experimental results. The structures located in the following energy profiles are all obtained through an optimisation procedure allowing for the total relaxation of all eight molecules.

3.2.1 Reaction profile for the 7:1:0 cluster:

The NH_3 and CO_2 reaction is investigated in the presence of six surrounding ammonia molecules. The energy profile is shown in Fig. 9:

The energy profile shown in this figure reveals four stable structures. The first one, R, can be viewed as the solvation of CO_2 in an ammonia solvent. It is characterised by a CN bond of 2.8 *Å*, associated with a frequency of 119 cm^{-1}. This system has to overcome a barrier of 6.3 kJ.mol^{-1} to produce the $NH_3^+CO_2^-$ zwitterion, Z, surrounded by six NH_3 molecules. The transfer of a proton from the zwitterion to a neighbouring ammonia leads to the formation of the carbamate anion C ($NH_2CO_2^-$) stabilised by the NH_4^+ ammonium cation. This transformation involves a barrier that is 11. kJ.mol^{-1} above R. Such a small barrier is consistent with the 5.1 kJ.mol^{-1} barrier found experimentally. Structure C is very stable with respect to R, *i.e.* 42. kJ.mol^{-1} below. One further hydrogen transfer can transform this carbamate anion to the carbamic acid, A. This transformation involves barriers of 13. kJ.mol^{-1} below R and 29. kJ.mol^{-1} above C.

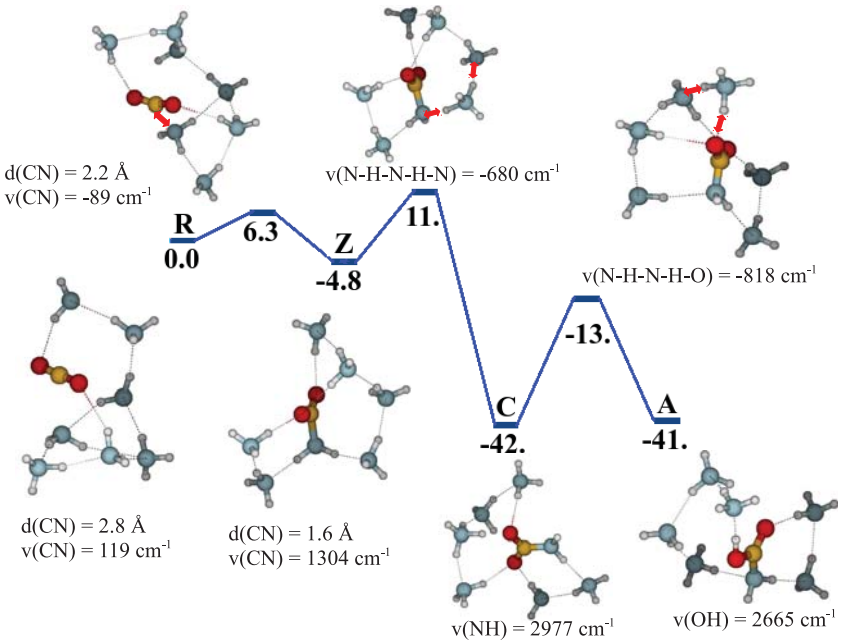

Fig. 9 B3LYP/6-311G(d,p) lowest energy profile for the formation of ammonium carbamate and carbamic acid in the 7:1:0 cluster. Energies are given in kJ.mol^{-1} and are corrected for unscaled zero-point energies. Green=carbon, red=oxygen, white=hydrogen. The arrows indicate the atomic motion during the reaction. R, Z, C, and A stand for reactants, zwitterion, carbamate anion, and carbamic acid structures, respectively. All relative energies are given with respect to R.

3.2.2 Reaction profile for the 1:1:6 cluster:

The reaction of NH_3 and CO_2 is investigated in the presence of six surrounding water molecules. The energy profile is shown in Figure 10:

The energy profile shown in Fig. 10 reveals three stable structures. As in the previous 7:1:0 structure, R can be viewed as CO_2 and NH_3 solvated in water. The CN bond of 2.6 *Å*, associated with a frequency of 160 cm^{-1}, is also consistent with the one obtained for R in the 7:1:0 structure. The second stable structure Z corresponds to the NH_3^+ CO_2^- zwitterion surrounded by six H_2O molecules. A water-mediated proton transfer involving a high barrier of 55 kJ.mol^{-1} above R leads to the formation of carbamic acid. Such a high barrier for the formation of NH_2COOH is certainly large, but this formation pathway will dominate if H_2O is more abundant than NH_3, as long as the temperature is high enough.

3.2.3 Reaction profile for the 2:1:5 cluster:

The reaction of NH_3 and CO_2 is investigated in the presence of five water and one NH_3 molecules The energy profile is shown in Fig. 11.

As for the previous energy profiles, structure R can be viewed as the solvation of CO_2 and NH_3 in a five water- and one ammonia-cluster. It is characterised by a CN distance of 2.6 *Å* with a frequency of 154 cm^{-1}, consistent with the two previous optimised R structures. The formation from R of Z2, a $NH_3^+CO_2^-$ zwitterion surrounded by five water and one ammonia molecules, involves a very small barrier of 4.6 kJ.mol^{-1}. A water-mediated proton transforms this zwitterion to a carbamate anion stabilised by a NH_4^+. The barrier for the transformation of Z2 to C is 5.0 kJ.mol^{-1} above R. Structure C is very stable with respect to R, *i.e.* 31. kJ.mol^{-1} below. This 5.0 kJ.mol^{-1} barrier for a mixed NH_3:H_2O solvation is lower than the 11. kJ.mol^{-1} barrier for a pure NH_3 solvation. The formation of the carbamate anion seems to be better catalysed by water than ammonia, if water and ammonia are both present. This is due to a higher efficiency of proton transfers. This phenomenon was not observed in the experiments in Section 3.1.3, but is clearly evident from the theoretical calculations.

A water-mediated proton transfer can allow for the transformation of this carbamate anion to the carbamic acid, A1. The transition state involved in the C $\rightarrow$ A1 transformation is lower in energy with respect to R by 23. kJ.mol^{-1}. This transition state is 8. kJ.mol^{-1} above C.

An alternative pathway has been investigated from another zwitterionic structure, Z1, although Z1 is close enough to Z2 that a simple relaxation can transform one into the nother. We found this zwitterion to transform to carbamic acid, A2, without going through the formation of a carbamate anion. This

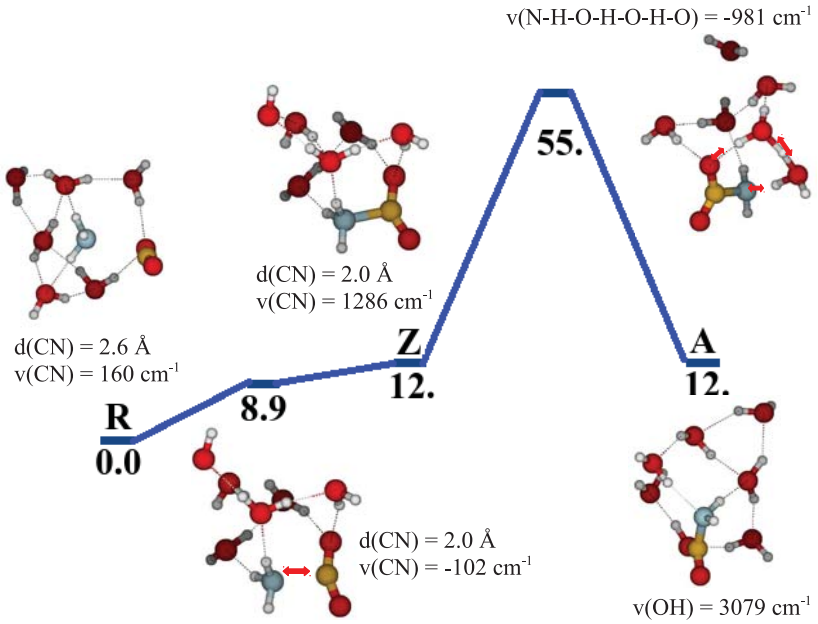

Fig. 10 B3LYP/6-311G(d,p) lowest energy profile for the formation of carbamic acid in the 1:1:6 cluster. Energies are given in kJ.mol^{-1} and are corrected for unscaled zero-point energies. Green=carbon, red=oxygen, white=hydrogen. The arrows indicate the atomic motion during the reaction. R, Z, A stand for reactants, zwitterion, and carbamic acid structures, respectively. All relative energies are given with respect to R.

transformation does, however, involve a high barrier of 39 kJ.mol^{-1} with respect to R. The barrier involved in the formation of A2 is much higher than the one involved in the formation of A1, both structures corresponding to carbamic acid but with a different arrangement of the solvent molecules. The reaction pathway via the carbamate anion structure should therefore be strongly favoured.

4 Discussion

On the basis of laboratory experiments and *ab initio* calculations we discuss the NH_2COOH and $NH_4^+NH_2COO^-$ formation mechanisms from a low temperature solid-phase NH_3 and CO_2 ice mixture. The mechanisms involved in the formation of the carbamate anion and the carbamic acid are concentration dependent.

In a CO_2-dominated ice, the proton transfer can not take place and no reactivity occurs.

In a protic environment, *i.e.* a NH_3- or H_2O-dominated ice, the less energetic pathway is the formation of the $NH_4^+NH_2COO^-$ carbamate, via the formation of a zwitterion (scenario 2). The carbamate then transforms into carbamic acid, according to:

$$\begin{aligned} NH_3 + CO_2 &\rightleftharpoons NH_3^+COO^- \\ NH_3 + NH_3^+COO^- &\rightleftharpoons NH_4^+NH_2COO^- \\ NH_4^+NH_2COO^- &\rightleftharpoons NH_3 + NH_2COOH. \end{aligned}$$

The formation of carbamic acid involves lower energy barriers when formed from the carbamate anion. The direct formation of carbamic acid is possible but energetically unfavourable. However, in a H_2O dominated ice, where there is a shortage of NH_3 reactants, this energetic pathway is the only one available. Calculations show that the carbamate seems to be better catalysed by water than by ammonia, although such a difference was not observed experimentally using kinetic experiments.

In a NH_3-dominated ice, the kinetics of the reaction are partial first-order with respect to CO_2 and partial zeroth-order with respect to NH_3 (for a NH_3 molar fraction between 0.5 and 1). The kinetic equation for the reaction can therefore be written as:

$$\frac{d(NH_4^+NH_2COO^-)}{dt} = -\frac{d(CO_2)}{dt} = k(T) \times (CO_2) \qquad (17)$$

The temperature dependence of the first-order rate constant is experimentally determined to follow an Arrhenius law, $k(T)=0.09^{+1.1}_{-0.08}$ s^{-1} $\times \exp(5.1 \pm 1.6$ kJ.mol$^{-1}/RT)$, in the

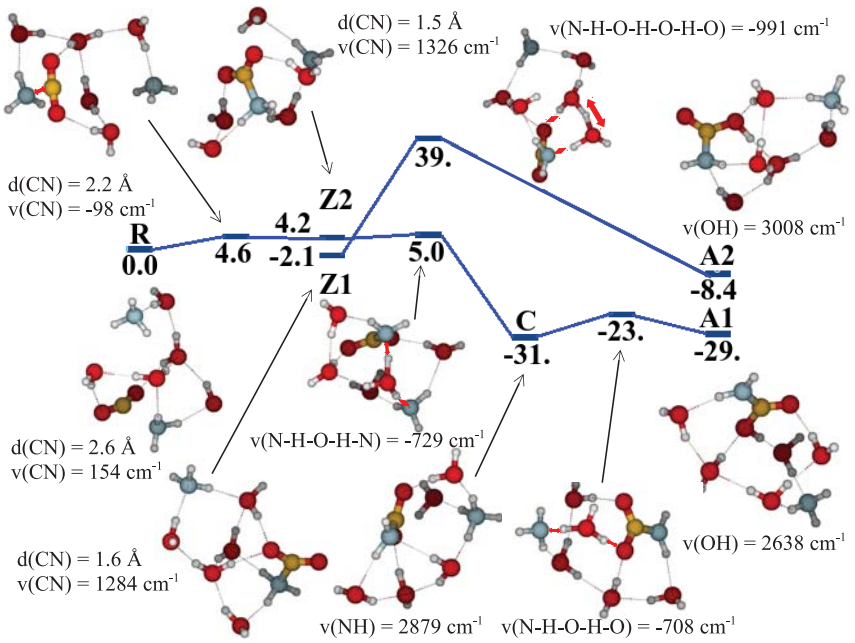

Fig. 11 B3LYP/6-311G(d,p) lowest energy profile for the formation of carbamate anion and carbamic acid in the 2:1:5 cluster. Energies are given in kJ.mol^{-1} and are corrected for unscaled zero-point energies. Green=carbon, red=oxygen, white=hydrogen. The arrows indicate the atomic motion during the reaction. R, Z1, Z2, C and A stand for reactants, zwitterions 1 and 2, carbamate anion, and carbamic acid structures, respectively. All relative energies are given with respect to R.

range 70 K to 90 K, when the reactants are located on two neighbouring sites, *i.e.* for a NH_3:H_2O ratio greater than 1:1.

The determination of the reaction barrier of the two reactants located on two neighboring sites is very important for later studies of diffusion-limited reactions. Indeed, solid-phase reactions in water-dominated ice, in either interstellar or atmospheric environments, are diffusion-limited[42]. The reaction will involve reactants either initially located on neighbouring sites (for a NH_3:H_2O ratio greater than 1) or brought to neighbouring sites by diffusion (NH_3:H_2O ratio lower than 1). The chemical reaction kinetics must be coupled with the diffusion kinetics of the reactants in order to fully describe such diffusion-limited reaction kinetics.

As shown in Fig. 12, the necessary diffusion of the reactants in H_2O-dominated ice ((NH_3:H_2O ratio lower than 1) slows down the kinetics of the NH_3 and CO_2 solid-state reaction. Very few studies exist on surface and volume diffusion in either crystalline[43,44] or amorphous ice[45,46]. Such studies on the diffusion of molecules in ice are a fundamental step toward the understanding of the kinetics of diffusion-limited reactions in ice. The coupling between solid-phase reactivity and diffusion in ice is therefore far from being understood.

We have also shown that $NH_4^+NH_2COO^-$ has a zeroth-order desorption rate constant, $k_{des}(T)=10^{13}s^{-1} \times \exp(69.0\pm 0.2$ kJ.mol^{-1}/(R$\times$ T)), and is therefore more refractory than water ice, which has a desorption energy of 46.6 kJ.mol^{-1} [47]).

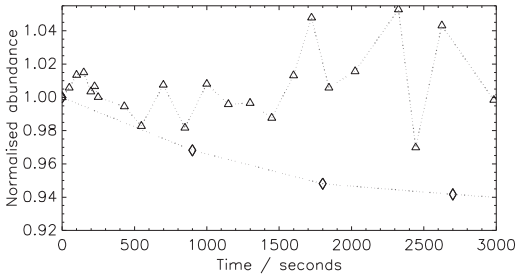

Fig. 12 Isothermal decay at 80 K of CO_2 in a CO_2:NH_3 ice film (diamonds) and in a CO_2:NH_3:H_2O ice film where H_2O is in excess with respect to NH_3 (triangles). The need for reactants to diffuse before reacting dramatically slows down the reaction.

This implies that some $NH_4^+NH_2COO^-$ can stay on the substrate (silicate, carbon, aerosol) surface at high temperature when water ice has sublimated. Such refractory species enter the composition of a residue, where a water-free chemistry can take place at higher temperature than the water ice sublimation temperature. For example, the reaction between amines and CO_2 produces alkyl-ammonium alkyl-carbamates which, under (solar or interstellar) ultraviolet irradiation, can lead to the formation of amino acid salts, such as ethyl-ammonium glycinate[34].

More generally, carbamates are CO_2 reservoirs. They can

store CO_2, which can be released at higher temperatures when the carbamate sublimates, as seen in Fig. 7. The rate of carbamate formation is important when calculating the overall rate of CO_2 removal. Carbamates can also be reaction intermediates in the synthesis of urea from NH_3 and CO_2 carried out in industrial plants[48]. Industrial research is presently carried out on methods of CO_2 removal in aqueous ammonia solutions[49]. At middle latitudes, the tropopause temperature ranges from an average of 15^{o}C at sea level to about -55^{o}C at the top of the tropopause. The NH_3 to NH_4^+ conversion rates has been estimated at between $10^{-3}s^{-1}$ [50] and $5\times10^{-5}s^{-1}$ [51]. Extrapolating the rate we have measured to these temperatures, we find reaction rates between 0.01 s^{-1} and 5 10^{-3} s^{-1}, with an average of 7 10^{-3} s^{-1}. This extrapolation is tentative since the temperature ranges are different. However, as long as diffusion is not involved, the amorphous or crystalline state of the ice should not be an issue. Our results are slightly higher than the previous estimates of the rate of removal of atmospheric gas-phase NH_3 and its transformation into (NH_4^+) salts aerosols. This can be explained by the effect of the diffusion on the overall reaction rate, as shown in Fig. 12.

5 Conclusion

We studied, both theoretically and experimentally, the low temperature solid-phase reactivity of the CO_2:NH_3 system. While NH_3 and CO_2 do not react in the gas-phase, we have shown that once in the solid-phase, the molecular environment can lower the reaction barrier, enabling the reaction between frozen CO_2 and NH_3 to occur. In a CO_2 dominated environment, the reaction is not possible. In a hydrogen bonded environment, such as in the presence of NH_3 or H_2O, the reaction barrier is lowered and the reaction is possible. The reaction produces both carbamic acid (NH_2COOH) and ammonium carbamate ($NH_4^+NH_2COO^-$). However the formation of $NH_4^+NH_2COO^-$ precedes the formation of NH_2COOH. The reaction can occur at temperatures below the desorption of the reactants, and its kinetic parameters can be measured using isothermal kinetic experiments and temperature programmed reactivity experiments on CO_2:NH_3 ice films. We concluded that the reaction rate constant follows an Arrhenius law $k(T)=0.09^{+1.1}_{-0.08}s^{-1}\times\exp(5.1\pm1.6\ \text{kJ.mol}^{-1}/(RT))$ between 70 K and 90 K. The product of this reaction, ammonium carbamate ($NH_4^+NH_2COO^-$), is more refractory than water ice and has a 69.0 ± 0.2 kJ.mol^{-1} first-order desorption energy for a $10^{13}s^{-1}$ pre-exponential factor. Carbamic acid (NH_2COOH) has a 76.1 ± 0.1 kJ.mol^{-1} first-order desorption energy for a $10^{13}s^{-1}$ pre-exponential factor. Real ices are water dominated, and thus solid-phase thermal reactions are diffusion-limited. The next steps are therefore to investigate the kinetics of the diffusion of each reactant and the kinetics of the reactivity of the CO_2:NH_3:H_2O mixture where H_2O is dominant. Understanding how the reactivity is limited by the diffusion of the reactants is the key to understand ice chemistry.

Acknowledgements

We thank the PCMI (Physique et Chimie du Milieu Interstellaire) program and the CNES (Centre National d'Etudes Spatiales) for financial support, and the HPC resources from GENCI-[CCRT/CINES/IDRIS] (grant 2014 [x2014085116]) for computing time. J.A.N. is a Royal Commission for the Exhibition of 1851 Research Fellow.

References

1 S. Krupa, *Environmental Pollution*, 2003, **124**, 179–221.
2 J. G. J. Olivier, A. F. Bouwman, K. W. Van der Hoek and J. J. M. Berdowski, *Environmental pollution*, 1998, **102**, 135–148.
3 J. Bassham, A. Benson and M. Calvin, *J. Biol. Chem.*, 1950, **185**, 781–787.
4 D. B. Dell Amico, F. Calderazzo, L. Labella, F. Marchetti and G. Pampaloni, *Chem. Rev.*, 2003, **103**, 3857–3897.
5 G. Sartori and D. Savage, *Industrial & Engineering Chemistry Fundamentals*, 1983, **22**, 239–249.
6 K. Hiraoka, A. Yamashita, Y. Yachi, K. Aruga, T. Sato and H. Muto, *The Astrophysical Journal*, 1995, **443**, 363–370.
7 Y. Oba, N. Watanabe, A. Kouchi, T. Hama and V. Pirronello, *The Astrophysical Journal Letters*, 2010, **712**, L174–L178.
8 S. Ioppolo, Y. van Boheemen, H. M. Cuppen, E. F. van Dishoeck and H. Linnartz, *Mon. Not. Roy. Astron. Soc.*, 2011, **413**, 2281–2287.
9 J. A. Noble, F. Dulieu, E. Congiu and H. J. Fraser, *The Astrophysical Journal*, 2011, **735**, 121.
10 M. Minissale, E. Congiu, G. Manicò, V. Pirronello and F. Dulieu, *Astronom.Astrophys.*, 2013, **559**, A49.
11 K. Hiraoka, T. Miyagoshi, T. Takayama, K. Yamamoto and Y. Kihara, *The Astrophysical Journal*, 1998, **498**, 710.
12 S. Ioppolo, H. M. Cuppen, C. Romanzin, E. F. van Dishoeck and H. Linnartz, *The Astrophysical Journal*, 2008, **686**, 1474–1479.
13 Y. Oba, N. Watanabe, T. Hama, K. Kuwahata, H. Hidaka and A. Kouchi, *The AstrophysicalJournal*, 2008, **686**, 1474–1479.
14 F. Dulieu, L. Amiaud, E. Congiu, J.-H. Fillion, E. Matar, A. Momeni, V. Pirronello and J. L. Lemaire, *Astronom. Astrophys.*, 2010, **512**, A30.
15 H. Mokrane, H. Chaabouni, M. Accolla, E. Congiu, F. Dulieu, M. Chehrouri and J. L. Lemaire, *The Astrophysical Journal Letters*, 2009, **705**, L195–L198.
16 E. Dartois, *Space Science research*, 2005, **119**, 293–310.
17 D. L. Frasco, *J. Chem. Phys.*, 1964, **41**, 2134–2140.
18 I. Hisatsune, *Canadian Journal of Chemistry - Revue Canadienne de Chimie*, 1984, **62**, 945–948.
19 J. B. Bossa, P. Theulé, F. Duvernay, F. Borget and T. Chiavassa, *Astronom. Astrophys.*, 2008, **492**, 719–724.
20 Y. Rodriguez-Lazcano, B. Mate, V. J. Herrero, R. Escribano and O. Galvez, *Phys. Chem. Chem. Phys.*, 2013, –.
21 Y.-J. Chen, M. Nuevo, J.-M. Hsieh, T.-S. Yih, W.-H. Sun, W.-H. Ip, H.-S. Fung, S.-Y. Chiang, Y.-Y. Lee, J.-M. Chen and C.-Y. R. Wu, *Astronom. Astrophys.*, 2007, **464**, 253–257.
22 R. K. Khanna and M. H. Moore, *Spectrochimica Acta Part A: Molecular Spectroscopy*, 1999, **55**, 961–967.

23 V. Bordalo, E. F. da Silveira, X. Y. Lv, A. Domaracka, H. Rothard, E. Seperuelo Duarte and P. Boduch, *The Astrophysical Journal*, 2013, **774**, 105.

24 M. Bertin, I. Martin, F. Duvernay, P. Theule, J. B. Bossa, F. Borget, E. Illenberger, A. Lafosse, T. Chiavassa and R. Azria, *Physical Chemistry Chemical Physics*, 2009, **11**, 1838.

25 P. Jackson, A. Beste and M. I. Attalla, *Phys. Chem. Chem. Phys.*, 2012, **14**, 16301–16311.

26 P. Theule, F. Duvernay, A. Ilmane, T. Hasegawa, O. Morata, S. Coussan, G. Danger and T. Chiavassa, *Astronom. Astrophys.*, 2011, **530**, A96.

27 T. Bartels-Rausch, V. Bergeron, J. H. E. Cartwright, R. Escribano, J. L. Finney, H. Grothe, P. J. Gutiérrez, J. Haapala, W. F. Kuhs, J. B. C. Pettersson, S. D. Price, C. I. Sainz-Diaz, D. J. Stokes, G. Strazzulla, E. S. Thomson, H. Trinks and N. Uras-Aytemiz, *Rev. Mod. Phys.*, 2012, **84**, 885–944.

28 F. Mispelaer, P. Theule, F. Duvernay, P. Roubin and T. Chiavassa, *Astronom. Astrophys.*, 2012, **540**, A40.

29 O. Kerkhof, W. A. Schutte and P. Ehrenfreund, *Astronom. Astrophys.*, 1999, **346**, 990–994.

30 H. Yamada and W. B. Person, *J.Chem.Phys.*, 1964, **41**, 2478–2487.

31 P. A. Gerakines, W. A. Schutte, J. M. Greenberg and E. F. van Dishoeck, *Astronom. Astrophys.*, 1995, **296**, 810.

32 S. A. Sandford and L. J. Allamandola, *The Astrophysical Journal*, 1990, **355**, 357–372.

33 J. B. Bossa, P. Theule, F. Duvernay and T. Chiavassa, *The Astrophysical Journal*, 2009, **707**, 1524–1532.

34 J.-B. Bossa, F. Duvernay, P. Theulé, F. Borget, L. D'Hendecourt and T. Chiavassa, *Astronom. Astrophys.*, 2009, **506**, 601–608.

35 S. A. Sandford and L. J. Allamandola, *The Astrophysical Journal*, 1993, **417**, 815–825.

36 O. Gálvez, I. K. Ortega, B. Maté, M. A. Moreno, B. Martín-Llorente, V. J. Herrero, R. Escribano and P. J. Gutiérrez, *Astronom. Astrophys.*, 2007, **472**, 691–698.

37 A. D. Becke, *J. Chem. Phys.*, 1993, **98**, 5648–5652.

38 P. J. Stephens, F. J. Devlin, C. F. Chabalowski and M. J. Frisch, *J. Phys. Chem.*, 1994, **98**, 11623–11627.

39 M. J. Frisch, G. W. Trucks, H. B. Schlegel, G. E. Scuseria, M. A. Robb, J. R. Cheeseman, G. Scalmani, V. Barone, B. Mennucci, G. A. Petersson, H. Nakatsuji, M. Caricato, X. Li, H. P. Hratchian, A. F. Izmaylov, J. Bloino, G. Zheng, J. L. Sonnenberg, M. Hada, M. Ehara, K. Toyota, R. Fukuda, J. Hasegawa, M. Ishida, T. Nakajima, Y. Honda, O. Kitao, H. Nakai, T. Vreven, J. A. Montgomery, Jr., J. E. Peralta, F. Ogliaro, M. Bearpark, J. J. Heyd, E. Brothers, K. N. Kudin, V. N. Staroverov, R. Kobayashi, J. Normand, K. Raghavachari, A. Rendell, J. C. Burant, S. S. Iyengar, J. Tomasi, M. Cossi, N. Rega, J. M. Millam, M. Klene, J. E. Knox, J. B. Cross, V. Bakken, C. Adamo, J. Jaramillo, R. Gomperts, R. E. Stratmann, O. Yazyev, A. J. Austin, R. Cammi, C. Pomelli, J. W. Ochterski, R. L. Martin, K. Morokuma, V. G. Zakrzewski, G. A. Voth, P. Salvador, J. J. Dannenberg, S. Dapprich, A. D. Daniels, . Farkas, J. B. Foresman, J. V. Ortiz, J. Cioslowski and D. J. Fox, *Gaussian 09 Revision D.01*, Gaussian Inc. Wallingford CT 2009.

40 R. L. Brown, *Journal of Research of the National Bureau of Standards*, 1981, **86**, 357–359.

41 S. A. Sandford and L. J. Allamandola, *Icarus*, 1990, **87**, 188–192.

42 P. Theulé, F. Duvernay, G. Danger, F. Borget, J. B. Bossa, V. Vinogradoff, F. Mispelaer and T. Chiavassa, *Advances in Space Research*, 2013, **52**, 1567–1579.

43 F. Livingston, J. Smith and S. George, *Journal of Physical Chemistry A*, 2002, **106**, 6309–6318.

44 C. A. Varotsos and R. Zellner, *Atmospheric Chemistry and Physics*, 2010, **10**, 3099–3105.

45 F. Mispelaer, P. Theulé, H. Aouididi, J. Noble, F. Duvernay, G. Danger, P. Roubin, O. Morata, T. Hasegawa and T. Chiavassa, *Astronom. Astrophys.*, 2013, **555**, A13.

46 L. J. Karssemeijer, S. Ioppolo, M. C. van Hemert, A. van der Avoird, M. A. Allodi, G. A. Blake and H. M. Cuppen, *Astrophys. Journal*, 2014, **781**, 16.

47 H. J. Fraser, M. P. Collings, M. R. S. McCoustra and D. A. Williams, *Month.Not.Roy.Astr.Soc.*, 2001, **327**, 1165–1172.

48 F. Barzagli, F. Mani and M. Peruzzini, *Green Chem.*, 2011, **13**, 1267–1274.

49 Z. Niu, Y. Guo, Q. Zeng and W. Lin, *Industrial & Engineering Chemistry Research*, 2012, **51**, 5309–5319.

50 A. Vermetten, W. Asman, E. Buijsman, J. Mulder W. and, Slanina and A. Waijers-Ijpelaan, *Verein Deutscher Ingenieure-Berichte*, 1985, **560**, 241–251.

51 J. Erisman, A. Vermetten, W. Asman, A. Waijers-Ijpelaan and S. J., *Atmospheric Environment*, 1988, **22**, 1153.